Journal of Power Sources 213 (2012) 358–374

Contents lists available at SciVerse ScienceDirect

Journal of Power Sources

journal homepage: www.elsevier.com/locate/jpowsour

Feasibility study for SOFC-GT hybrid locomotive power part II. System packaging and operating route simulation

Andrew S. Martinez, Jacob Brouwer*, G. Scott Samuelsen

National Fuel Cell Research Center, University of California, Irvine, CA 92697-3550, USA

ARTICLE INFO

Article history:
Received 21 January 2012
Received in revised form
10 April 2012
Accepted 12 April 2012
Available online 24 April 2012

Keywords:
SOFC-GT
Locomotive
Diesel
Dynamic simulation
packaging
Carbon dioxide

ABSTRACT

This work assesses the feasibility of Solid Oxide Fuel Cell-Gas Turbine (SOFC-GT) hybrid power systems for use as the prime mover in freight locomotives. The available space in a diesel engine-powered locomotive is compared to that required for an SOFC-GT system, inclusive of fuel processing systems necessary for the SOFC-GT. The SOFC-GT space requirement is found to be similar to current diesel engines, without consideration of the electrical balance of plant. Preliminary design of the system layout within the locomotive is carried out for illustration. Recent advances in SOFC technology and implications of future improvements are discussed as well. A previously-developed FORTRAN model of an SOFC-GT system is then augmented to simulate the kinematics and power notching of a train and its locomotives. The operation of the SOFC-GT-powered train is investigated along a representative route in Southern California, with simulations presented for diesel reformate as well as natural gas reformate and hydrogen as fuels. Operational parameters and difficulties are explored as are comparisons of expected system performance to modern diesel engines. It is found that even in the diesel case, the SOFC-GT system provides significant savings in fuel and CO_2 emissions, making it an attractive option for the rail industry.

1. Introduction

As discussed in Part I of this work, the transportation of goods by rail has historically been a major portion of the overall freight transportation system in the United States. Although its use declined for some years in favor of trucks, freight transport by rail has recently begun to be more widely utilized again and is now more prevalent than trucking, on a ton-mile basis [1]. Thus, it is reasonable to assume that transport by rail will continue to have a major role in our nation's freight-carrying infrastructure.

A complete understanding of the emissions impact of locomotives is still an active research area, but it is becoming increasingly clear that a significant stress is imparted on the environment and the health of those living near the rail lines' centers of operation. Recent studies carried out in the Southern California area highlight impacts on the population living near rail operations centers, caused mostly by the emission of diesel particulate matter (PM). In one year, these PM emissions from the Ports of Los Angeles and Long Beach have been estimated to be responsible for 29 deaths, 750 asthma attacks, and as many as 6600 lost work days [2]. Another study at the BNSF rail yard in San Bernardino, California found that in the neighborhoods nearest to the rail yard, the risk of lung cancer was nearly double the background risk; nearly 36,000 residents living within one mile of the rail yard were estimated to have an increased cancer risk between 10 and 50% of the background [3]. Clearly, the current locomotive-based emission of PM proves to be a concern, with a significant environmental justice impact.

In addition to PM emissions are concerns regarding fuel efficiency, fuel cost, and emissions of greenhouse gases, including CO_2 in particular. It is estimated that one gallon of diesel fuel typically produces 10,217 g of CO_2 [4]. In 2005, 5714 trillion BTUs of diesel fuel were utilized by the freight rail industry, or approximately 4.44 billion gallons [5]. This represents a potential emission of 45.36 million tons, or approximately 7.4% of the total national emission of CO_2 in the same year [6]. Given the current emphasis on reduction in Greenhouse Gas emissions, it is reasonable to assume that locomotives may be required to reduce their GHG emissions. In addition, there is evidence that the industry is moving forward with plans to address the concern, as the development of General Electric's Evolution and Evolution Hybrid locomotives seem to indicate [7–9]. Moreover, current EPA guidelines provide restrictions on locomotive emissions of CO, unburned hydrocarbons, and NO_x, all of which have been discussed in Part I. The consideration of the

* Corresponding author. Tel.: +1 949 824 1999; fax: +1 949 824 7423.
E-mail address: jb@nfcrc.uci.edu (J. Brouwer).

0378-7753/$ – see front matter © 2012 Elsevier B.V. All rights reserved.
doi:10.1016/j.jpowsour.2012.04.023

impact of diesel fuel use and emissions signature from the rail industry provide strong motivating factors for the investigation into alternative systems for powering the industry's locomotives.

Thus, the need for more locomotives with a smaller environmental impact has been recognized. Given how thoroughly the diesel engine has penetrated the locomotive market as the engine technology of choice, the development of strategies to improve diesel technology is a logical first step for improving the fuel efficiency and emissions characteristics of locomotives. However, future efficiency and emissions requirements may exceed the capabilities of diesel technology requiring an investment in new technologies and capabilities that may be applicable to the railway prime mover. Early investment in emerging technologies, such as solid oxide fuel cells, may provide more options and open the door to greater improvements. The fuel cell has already been identified as having an opportunity to completely replace the entire diesel and electric power system for a locomotive [10].

Research to-date has nearly exclusively considered low-temperature fuel cells in this application. Application-based research for high-temperature fuel cells has additionally focused on stationary power applications. In spite of this focus, the locomotive application of fuel cells has been studied since the 1980's, especially in the context of use for the Canadian rail system [11–13]. Although the particular fuel cell type, fuel, and system configurations varied, these early models and studies did conclude that the use of a fuel cell system in this application was possible, and could have substantial benefits, but that the economic viability was a hurdle which would have to be overcome. These findings are common to many previous fuel cell systems analyses, especially given the early stage of development of fuel cell technologies and the lack of mass production capability for this technology. Scott et al. further emphasized that life-cycle considerations made the option more competitive [14]. Their conclusions also pointed to increased viability in the case of possible levies based on emission rates.

Significant investment in the practical application of fuel cells to American railway applications has been accomplished by Vehicle Projects, LLC. In 2002, Vehicle Projects developed the first fuel cell locomotive, building a 17 kW mine cart for use in Ottawa. Vehicle Projects are currently nearing completion of a fuel cell-battery hybrid switcher locomotive, based on the design of a diesel-battery hybrid. The Department of Defense is also working with Vehicle Projects to develop a 1.2 MW locomotive that is designed for freight transport but can also be utilized as a base power plant, thereby providing dispatchable emergency power for the military [12]. The design process for the near-complete railyard switcher locomotive has been well-documented, including much discussion of feasibility and physical constraints [15–17]. The wide range of interests and attention to detail in many of these investigations is a positive indicator of the applicability, potential, and interest in this technology.

Note that all of the above studies and developments have only considered low-temperature fuel cells, primarily using PEM technology. This may be due to a need for quick startup in these applications or may be motivated by the desire to study a fuel cell type of a particular industrial partner or that is closer to commercialization and mass production. Regardless of the motivation, there has consistently been some concern about the power density of the fuel cell system, as there is limited space available on a locomotive for the prime mover, and fuel cells tend to have lower power density than diesel engines. PEM fuel cells have traditionally had the highest power density of any fuel cell type. However, recent SOFC developments suggest that SOFC technology can achieve very high power density [18]. In addition, SOFCs are expected to have higher efficiency (lower polarizations) and are inherently much more fuel-flexible, which could reduce the size requirements of the onboard fuel and fuel processing system, further alleviating the physical constraints on the system.

Further integrating the SOFC with a gas turbine to create a hybrid SOFC-GT system could provide even greater efficiency and power density, as typical combined efficiencies of such systems are higher than SOFC systems alone, surpassing 70% [19,20]. In addition, the use of diesel fuel, enabled by SOFC fuel flexibility, will aid in the transition to a new engine technology and will support higher fuel energy density compared to hydrogen. SOFC technology has proven high efficiency and low emissions, which can alleviate concerns about fuel use and environmental impact. All of these factors support the consideration and motivate the analysis of a diesel-fueled SOFC-GT locomotive engine. The current novel analysis is intended to determine whether or not recent advances in SOFC-GT technology enable it to positively contribute to clean and efficient future freight rail applications. In this work, this analysis is presented as a two-part process: first, the physical constraints on the sizing of the system are examined, followed by an investigation into the operational capability of the system. Similar to Part I, the simulations in this work do not yet consider the integration of the reformer, but analyze a scenario in which fossil fuel reformates are generated offboard and supplied to the locomotive fuel tank.

2. Calculations for physical constraints

2.1. Satisfying space constraints

A major consideration for the feasibility of an SOFC-GT system applied to locomotive power is to determine whether there is sufficient space available in the engine compartment of a current locomotive design. The integration of the SOFC-GT system should be as seamless as possible; thus, it would be undesirable to use multiple locomotives to provide the same power as a single diesel engine-powered locomotive. In addition, it would be desirable for the fuel system to not impose a volumetric or mass constraint that would require pulling a fuel tender. All of the components necessary for the SOFC-GT unit, fuel storage, and fuel processing systems, as well as balance of plant components are considered for placement within the confines of a typical locomotive engine compartment.

Diesel fuel is desired for operation of the SOFC-powered locomotive because it allows rail operators to continue to use a familiar fuel for which there exists a substantial and satisfactory infrastructure. Other fuels, such as bio-fuels, LNG, CNG, or even H_2 could be readily applied to future use; however, early introduction of such fuels is unlikely due to the additional challenges of establishing an entire fuel provision infrastructure. In the long-term, SOFC technology could enable a transition to alternative fuel use in rail applications due to inherent fuel flexibility.

For reference, most of the comparisons in this work have been made to the AC4400CW and ES44AC/DC locomotives designed by GE and their associated GE7FDL and GEVO-12 (a modified GE7FDL) engines. The GE7FDL engine used on the AC4400CW is a 4500 hp (3355 kW) engine, weighing 19,736 kg, and measuring 4.90 m long by 1.74 m wide by 2.98 m tall, inclusive of the exhaust stack [21]. This 16-cylinder engine is replaced by the 12-cylinder, 4400 hp GEVO-12 on the ES44AC/DC, for which specifications are currently unavailable. However, the total engine compartment, which includes more than the diesel engine itself, provides a floor space of approximately 11 m^2 and a volume of around 53 m^3.

In this application, both volumetric and footprint constraints must be met, since overall locomotive width and height are limited by external infrastructure constraints such as tunnel dimensions.

The GE7FDL engine compartment effectively has an area-specific power density of 30.5 W cm^{-2} its volumetric power density is 0.063 W cm^{-3}. A conservative estimate of a modern planar SOFC single-cell power density is approximately 0.5 W cm^{-2} Assuming that the full 2.98 m of height is available to the SOFC stack, and that a typical cell repeat unit (including interconnects) is 5 mm thick, 596 cells could be placed into a single stack, yielding a stack area-specific power density of 298 W cm^{-2}, or 1 W cm^{-3}. On this basis, the SOFC stack is approximately an order of magnitude more power-dense on both a footprint and volumetric basis than the diesel engine, without accounting for balance of plant components such as manifolding, insulation, and heat exchangers.

Prior fuel cell-gas turbine systems have been designed with an 85:15 split in power produced from the fuel cell and gas turbine, respectively [22]. Assuming the same power split for the locomotive system, the SOFC would have to provide approximately 2900 kW, with the turbine providing just over 500 kW of power. To determine the size and weight specifications of applicable turbines, commercial designs in the range of 200–1200 kW were surveyed. The volume- and area-based power densities of several existing gas turbine engines are presented in Fig. 1. Integration of turbomachinery into a hybrid SOFC-GT cycle inevitably "derates" gas turbine power because the SOFC provides gases to the inlet of the turbine at temperatures significantly lower than the combustor of the original gas turbine design. Based on previous hybrid system designs, selecting a turbine rated at 1000 kW is then a reasonable expectation for the required gas turbine rating.

Such a turbine has approximately an area-specific power density of 11 W cm^{-2} and a volumetric power density of approximately 0.05 W cm^{-3}. The existing gas turbines in this range of size class are the 1000 kW Kawasaki GPS1250 M1A-01, with specifications of 12.0 W cm^{-2} and 0.048 W cm^{-3} [23], and the 1200 kW Solar Saturn 20, with specifications of 10.6 W cm^{-2} and 0.050 W cm^{-3} [24]. These values are lower than current locomotive diesel engines and the SOFC stack; therefore, the power split between the SOFC and GT plays an important role in the packaging feasibility of the SOFC-GT system. Thus, the overall power system would have the space breakdown shown in Table 1. In the calculations shown for the SOFC, the sizes of the stack ancillary equipment and balance of plant components have been accounted for as scaling factors, based on measurements of the stack and total system in an existing Siemens 25 kW SOFC. The footprint and volume factors were found to be 2.8 and 4.75, respectively.

The results presented in Table 1 suggest that it is feasible to produce a future hybrid SOFC-GT system that could fit within the operating envelope of a modern locomotive, if the fuel processing

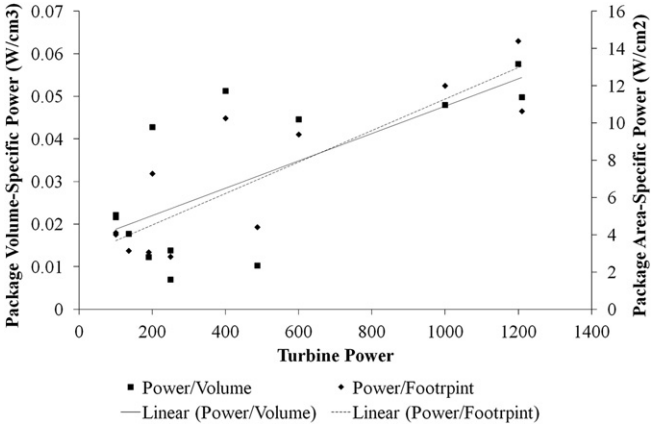

Fig. 1. Gas turbine size:power correlations.

Table 1
Calculated size specifications of a potential future SOFC-GT and standard diesel locomotive engines.

	Footprint (m^2)	Volume (m^3)
Total Diesel-Electric System	~11	~53
SOFC	2.70	13.55
GT	9.02	21.74
Total SOFC-GT System	11.72	35.29

can be moved offboard of the locomotive. However, to minimize the changes in day-to-day operation and make the integration of the SOFC-GT system as seamless as possible, the engine replacement would require the inclusion of an onboard fuel processing system. Assuming diesel fuel, two major reactors are required. The first is the autothermal reformation unit that converts the diesel into a hydrogen-rich stream. The second unit is the sulfur removal bed, most likely comprised of a ZnO bed that can absorb the sulfur from the H_2S molecules in the reformate stream.

A satisfactory index for estimating the fuel reformer size is the gas hourly space velocity (GHSV), relating the flow rate of the fuel to the total volume of the catalytic reactor. The volume of the required reactor can be estimated as:

$$V_{\text{ref}} = \frac{\text{H}_{2,\text{req}}}{\eta_{\text{conv}} \cdot \text{GHSV}} \tag{1}$$

where V_{ref} is the reformer reactor volume, $\text{H}_{2,\text{req}}$ is the required volumetric flow rate of hydrogen, and η_{conv} is the hydrocarbon-to-hydrogen conversion efficiency of the reformer reactor. The required hydrogen flow rate can be calculated as:

$$\text{H}_{2,\text{req}} = \frac{i}{nF\eta_{\text{FC}}u_{\text{FC}}} \cdot \frac{R_u T}{P} \tag{2}$$

where i is the total stack current, n is the number of electrons participating in the redox couple, F is Faraday's constant, η_{FC} is the fuel cell energy conversion efficiency, u_{FC} is the fuel cell fuel utilization, R_u is the universal gas constant, and T and P are the operating temperature and pressure of the fuel cell stack. Assuming operational parameters as in Table 2, the catalyst bed volume would have to be 3.87 m^3. The current was calculated assuming an approximately 3.5 MW system with a 0.7 V cell voltage, thereby providing a conservative, oversized reactor volume.

Sulfur removal beds are typically regenerable ZnO beds, which undergo a period of desulfurizing the feed stream followed by a period of oxidative regeneration. During regeneration, the sulfur absorbed to the catalyst becomes desorbed and forms sulfur oxide compounds. Due to the frequency of regeneration, the GHSV must account for the desired length of operation between regeneration cycles. Values for GHSV vary widely based on the material chosen

Table 2
Specifications of the integrated system for diesel reforming under overall autothermal conditions.

Parameter	Value	Units
η_{conv}	0.3	–
GHSV	2.78 (10,000)	s^{-1} (h^{-1})
I	5,000,000	A
N	2	mol
F	96,485	C-mol^{-1}
η_{FC}	0.3	–
u_{FC}	0.85	–
R_u	0.08205	L-atm-mol^{-1}-K^{-1}
T	773	K
P	2	atm

for the catalyst and the operating temperature. ZnO beds in available commercial and laboratory units typically operate around 2000–3000 h^{-1} [25–27]. At 4500 h^{-1}, it has been shown that a sulfur removal bed fed with fuel containing 1150 ppm sulfur could operate for more than 200 h before sulfur breakthrough occurs, necessitating regeneration of the ZnO bed [28]. This inlet sulfur concentration is higher than the current regulation of 500 ppm, and much higher than the 15 ppm that will be the new standard in 2012 [29]. High-temperature performance has also been demonstrated with lanthanum oxide sorbents and space velocities up to 400,000 h^{-1} with extremely small loss in sulfur absorption capability over repeated cycles [30]. Following full reactor size recommendations in this work, the potential would then exist for the sulfur removal unit required to occupy only 0.12 . Thus, assuming the sulfur and reformer units to be the same size provides a conservative estimate of 7.74 for the entire fuel processing system.

As shown in Table 3, the full system integration of SOFC-GT with fuel processor is roughly equivalent to the diesel standard, requiring a slightly larger footprint, but occupying less overall volume. With careful engineering, the footprint constraint should be achievable as well. Moreover, it should be remembered that this is considering a conservative SOFC power density as well as a power split that may be less than optimal; as Table 3 shows, the gas turbine presents even more of a challenge than the SOFC and fuel processing subsystem. A split in power rating further emphasizing SOFC may prove to make the system smaller; this consideration would have to be balanced with system power output and efficiency considerations. In addition, future advances in gas turbine design, which have not been considered here, could lead to smaller package size.

There also exists the opportunity to create more space for the SOFC-GT system by accounting for balance of plant components, such as the size of the power conditioning system. In addition, the sulfur removal step could be moved offboard, as a pre-treatment prior to filling the tank of the locomotive itself. A conceptual drawing of the SOFC-GT system with the assumption of the full fuel processing system onboard a locomotive's frame is presented in Fig. 2. The green, cylindrical units represent the two fuel processing reactors, the four maroon objects in the center represent SOFC stacks, and the large blue object on the right represents the gas turbine.

FC-GT systems developed and tested to-date have not demonstrated the high power density and small footprint of either the current diesel-electric system or the calculated potential SOFC-GT system. A few examples of commercial and research fuel cell and fuel cell-gas turbine systems are available in the literature. Within the commercial sector, Fuel Cell Energy is the only company to-date that has demonstrated a commercially-available fuel cell-gas turbine product. Their DFC 3000, a 2800 kW molten carbonate fuel cell (MCFC) stationary power unit, requires a footprint of approximately 368 m^2 and a volume of 2800 m^2 [31]. Their DFC-T, a 2300 kW MCFC-GT unit, occupies 181 m^2 and 1150 m^3, thereby showing little advantage in system size by hybridizing a fuel cell system with a turbine [32]. Several considerations may be

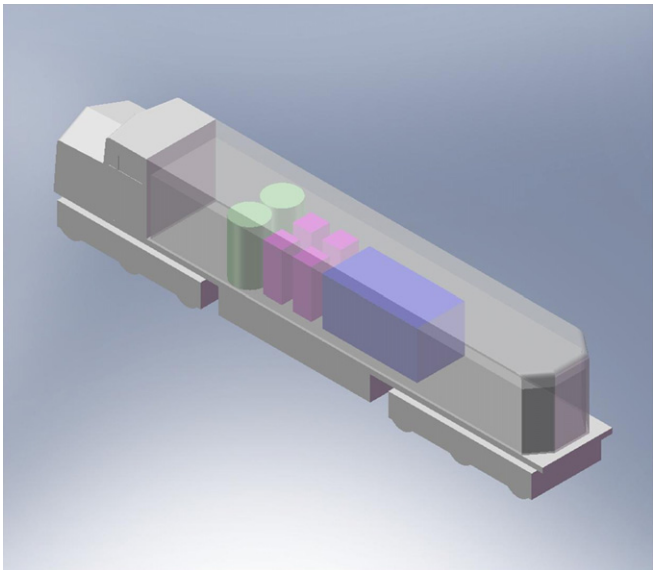

Fig. 2. Conceptual layout for SOFC-GT prime mover aboard a locomotive.

responsible for the large size of these systems: (1) these systems are based upon the low current density capability of molten carbonate fuel cells, (2) MCFC have poor overall power density compared to modern SOFC, (3) MCFC require a very large balance of plant (primarily due to cathode recycle), and (4) the DFC-T system does not represent an optimal integration of FC and GT since it was based upon an existing FC and GT commercial system rather than two units that were specifically designed to work together.

Likewise, examples of SOFC and SOFC-GT systems do not meet the standards of current locomotive design. Measurements of a Siemens 25 kW system at the National Fuel Cell Research Center (NFCRC) show that it requires an overall footprint of 3.16 m^2 and a volume of 6.25 m^3. A 220 kW Siemens SOFC-GT system also demonstrated at the NFCRC with the cooperation of Southern California Edison occupied an area of 22.23 m^2 and had a volume of 77.7 m^3 [20]. This 220 kW system would require 47% more volume than the GE7FDL and provide less than one tenth the power of the current diesel engine. The resulting power density of the SOFC-GT system is only 5% of the GE7FDL on a volumetric basis; an SOFC-GT system with the same power output as the GE7FDL would have a footprint of 323 m^2 and a volume of 1184 m^3. Table 4 compares these systems to the conceptual SOFC-GT and current diesel-electric system on a per-unit footprint and volume basis, highlighting the orders of magnitude difference between the technology potential and demonstrated units.

These system specifications are not adequate for the locomotive application. Four major reasons for the large size of the 220 kW system in particular include: (1) it was a proof-of-concept system, (2) it was not optimized for practical application, (3) the fuel cell was not well matched to the available turbo-machinery, and (4) the fuel cell used tubular SOFC technology developed in the 1990s that

Table 3
Calculated size specifications of a fully integrated diesel fuel processor with SOFC-GT and comparison to a standard diesel locomotive engine.

	Footprint (m^2)	Volume (m^3)
Total Diesel-Electric System	~11	~53
SOFC	2.70	13.55
GT	9.02	21.74
Fuel Processing	3.16	7.74
Total SOFC-GT System	14.88	43.03

Table 4
Comparison of area- and volume-specific power densities of theoretical and demonstrated power systems.

	Footprint (W-cm^{-2})	Volume (W-cm^{-3})
SOFC-GT Theoretical	22.55	0.078
Total Diesel-Electric System	30.50	0.063
DFC 3000 MCFC (2800 kW)	0.76	0.001
DFC-T MCFC-GT (2300 kW)	1.27	0.002
Siemens SOFC (25 kW)	0.79	0.004
Siemens SOFC-GT (220 kW)	1.04	0.003

had very poor power density compared to modern planar cells. However, in all the example systems, they were designed to operate in stationary power applications; thus, the design process did not value power density (unlike transport fuel cell system designs). Moreover, the early development stage and the nature of the fuel cells used produced systems with fuel cell stacks larger than what is feasible with current anode-supported technology. Additionally, well-integrated and matched hybrid SOFC-GT systems should be able to significantly improve power density and footprint characteristics.

While planar anode-supported SOFC technology may significantly contribute to the feasibility of SOFC-GT use in locomotive applications, another possible technology for use in this application is micro-tubular SOFC. Winkler and Lorenz have noted that for the automotive transportation sector, recent advances in micro-tubular SOFCs, along with the continued reduction in size of MTGs without loss of efficiency, may be the keys to the practical feasibility of mobile SOFC-GT hybrid power systems [33]. One of the prominent research groups involved in micro-tubular SOFC is from the Institute of Advanced Industrial Science and Technology (AIST) in Japan, in cooperation with the New Energy and Industrial Technology Development Organization (NEDO). The group has developed micro-tubular SOFCs with diameters less than 1 mm, and lengths up to a few centimeters [34–39]. Development has progressed up to stack design, which relies on a cathode matrix as the interconnection between cells. The materials set is based upon use of a ceria electrolyte, which allows operation in the temperature range of 500–600 °C.

The advantages of using the micro-tubular cell design are cited as being two-fold [40]:

1) Because of the small size, there is a high ratio of active surface area to overall volume of the cell, resulting in stacks that are potentially high in volumetric power density. Observed power densities are 1 W/cm^2 using the traditional fuel cell definition, 8.7 W/cm^3 by extrapolation of cell design to a 25-cell 1 cm^3 stack operating at 570 °C.
2) The design of the tubular cell, along with the small size, allows for quick startup of the system. In addition, this startup does not place the cell in jeopardy of thermal fracture, due to the distribution of stresses in a tubular design.

Possible disadvantages include an unknown cost and therefore uncertain commercial viability, a reported issue with efficient current collection from the anode side of the cell [37], complex manifolding requirements, and unknown durability. In addition, in the application of an SOFC-GT system, the lower operating temperature of these cells may be disadvantageous. All reports from the group also cite a low OCV, which is most likely due to electrolyte electronic conductivity associated with ceria reduction. Although they have yet to demonstrate it, they point to the possibility of novel electrolytes (modified ceria-based structures) in order to raise the OCV [41,42].

The demonstrated volumetric power densities of micro-tubular SOFC have been on the order of 1 W cm^{-3}. Their goal for this phase is 2 W cm^{-3}, which would match the most advanced planar SOFC technology. However, estimates of the technology potential argue that power density could reach 4 or 7 W cm^{-3} at 500 and 550 °C, respectively [34]. Toward the demonstration of this performance, recent work detailed a stack with a 3-by-3 layout of cells that was operated at 484 °C and achieved a total output of 1 W, with a total stack volume of less than 1 cm^3 [40]. Other researchers have also investigated this technology, with a variety of approaches to achieving improved performance [43,44]. These results illustrate that the concept can achieve performance at least comparable to the feasibility calculations presented above. Therefore, in spite of the lack of demonstrated units, there is an abundance of factors available that indicate the theoretical feasibility of such a system.

2.2. Comparison of power system mass

System mass may also be a concern similar to occupied space. Although more weight may aide in traction considerations, it also causes increased power and efficiency loss. However, compared to the total mass of the entire train when the cars are included, the locomotive mass may be negligible. The GE7FDL engine has a specific power of 170 W/kg. The current SECA [18] target for SOFCs is 200 W/kg, the achievement of which would give the SOFC a weight advantage compared to the diesel engine. However, Sasaki et al. have reported that micro-tubular have specific power of 10,500 and 16,900 W/kg at 500 and 550 °C, respectively [38]. The potential exists for SOFC technology to exhibit specific powers far exceeding what is currently used in the locomotive's power unit. In By contrast, the Kawasaki turbine has a specific power of only 95.23 W/kg, much lower than the diesel engine. Assuming only the SECA goal for the SOFC power density and the incorporation of the Kawasaki turbine, the SOFC and GT unit masses are 14,260 kg and 9525 kg, respectively. Thus, the total power unit mass is approximately 23,800 kg, approximately 4.5 tons heavier than the current diesel engine. The relative importance of this additional mass may require detailed future study.

2.3. Additional hybrid system features for locomotive applications

Beyond the space limitations considered above, an SOFC-GT system demonstrates additional features worthy of consideration for use in long-haul locomotive applications. Not all of these are advantages compared to diesel engines since some are shared qualities, however the usefulness of these features should be considered potential benefits.

1) An SOFC is fuel-flexible and can operate on the diesel fuel already common in freight applications as well as on alternative fuels, including bio-fuels, LNG, CNG, and other hydrocarbons. This allows for a more viable transition from diesel fuel to hydrogen by allowing the industry to decide when it wishes to invest in new fueling infrastructure.
2) An SOFC is fundamentally modular and allows for replacement and repair of only those portions of the fuel cell system that are no longer functioning properly. Additionally, GT technology has proven reliability advantages compared to a reciprocating engine.
3) An SOFC-GT system has fewer moving parts than a diesel engine, which may allow it to produce less noise.
4) The exhaust temperature of the SOFC-GT could be available for high quality heat provision to other train uses. Fuel and air preheat, reformation thermal support, and adsorption chilling are all possible uses that can increase overall efficiency.

3. Modeling methodology to demonstrate operational capability

In Part I of this work, a detailed account of the development of a FORTRAN system model was provided. In addition, preliminary demonstrations of the ability of the model to provide performance predictions at steady-state and during simple load dynamics were provided along with some discussion of insights regarding the fundamental differences between operation on hydrogen, natural gas reformate, and diesel reformate. In this work, the same model was utilized to investigate a more rigorous, and more realistic, load

profile. However, there were some important changes made to the model during the development of these real-world scenarios.

3.1. Change in system layout

In the model developed for Part I of this investigation, the system only provided preheat of the air entering the fuel cell on the cathode side. In the system models provided for the simulations along an actual freight route, an additional fuel preheater has been added. This preheater was utilized to preheat only the fuel entering the anode of the fuel cell and was fed by exhaust air flowing out of the air preheater. Although the air preheater was previously described to be simulated as a counter-flow heat exchanger, it was found that the disparity in inlet heat rate flowing through the fuel and air sides of the fuel preheater provided a substantial numerical difficulty. Thus, the fuel preheater was instead modeled as a co-flow heat exchanger since this removed one level of iteration in the solution method and was numerically much simpler to solve.

3.2. Change in control methodology

In the previously-presented results, the control method and the control gains were not fine-tuned; they were simply structured and tuned to values that provided reasonable performance. Re-tuning was required in this work due to the more strenuous dynamic operation. Additionally, the structure of the controller had two modifications. The first change was that the control of the SOFC Average Temperature, previously denoted as Level 1, was not allowed to inhibit the progress of the controller to Level 2. Through experimentation with the controller, it was found that control of the cell cooling and fuel flow needed to occur simultaneously; thus, the restriction was eliminated. Additionally, control of the turbine inlet temperature previously allowed operation within a band of temperatures, and thus allowed auxiliary fuel flow rate to "float." However, this allowed system efficiency to drop over the course of simulation For example, if no auxiliary combustor fuel was flowing at rated power of 3.5 MW, then system power dropped to 875 kW, auxiliary fuel flow would increase to maintain the minimum turbine inlet temperature. However, if system power subsequently returned to 3.5 MW, the combustor fuel flow rate would float and overall system efficiency was negatively impacted. To rectify this, the combustor fuel flow rate was reduced at times when the system had come to steady-state and the turbine inlet temperature was above its minimum.

3.3. Addition of train kinematics and locomotive notching logic

Demonstrating the system's capabilities along a realistic freight route requires a description of the train kinematics and the engineer's notching logic. In this work, it is assumed that the train consists of 100 cars, fully loaded to the maximum allowable weight reported by Union Pacific [45], and six locomotives, with the placement of the locomotives as indicated in Fig. 3. It was additionally assumed that the length (allowing for extension of the couplers) and weight of the cars were 62.5 feet and 143 tons; the locomotives were assumed to be 165 feet long with a weight of 207.4 tons. A set of points (A–F) was tracked to determine if there was an inflection in the grade of the track anywhere along the length of the train. Given that the length of the train was approximately 1.37 miles and the features of the modeled route, it was only required to track for one inflection point along the train. The entirety of the train was thus treated at all times as two connected point masses experiencing varying forces as shown in Fig. 4.

At all times, there are several forces acting on each of the point masses. The first of these is the Tractive Effort, abbreviated TE, provided by either the power of the locomotives' energy systems or the power of the brakes. Due to the logic of the notching, at no time were the two tractive efforts allowed to act concurrently. The two tractive efforts in this model were calculated according to

$$\mathrm{TE}_{\mathrm{Power},i} = \frac{P_i}{V} \tag{3}$$

and

$$\mathrm{TE}_{\mathrm{Brake,Max},i} = \frac{L_i \cdot 3.5\mathrm{MW}}{V} \tag{4}$$

where P_i in Eq. (3) refers to the power contributed by all locomotives in mass i and V refers to the train velocity. A 15% loss was assumed in the conversion of power from the SOFC-GT system to the power applied at the wheels; thus P_i should not be confused for the developed system power. Eq. (4) provides an expression for the maximum braking tractive effort, which would only occur at the highest braking notch (to be discussed below); values at other braking notches would simply be a fraction of this maximum. The braking provided by tractive effort derives from the dynamic braking enabled by current motor designs, which allow their polarities to be switched and the motors to act as generators. This type of braking can only occur on the motors in the locomotive; thus, the term L_i in Eq. (4) is the number of locomotives in mass i. The energy absorbed through this braking action is typically dissipated through a large resistor or, if system design permits, stored in batteries. The current work assumes dissipation.

Braking tractive effort is not the only means of providing braking to the train. Typical train car designs provide air-powered caliper brakes at each car's wheel truck. It was assumed that an air-supplied braking system was also available aboard the train. The dynamic operation of these systems is often complex, with the train engineer managing system pressure as it is released during braking periods and slowly replenished during times between application of the brakes. In this work, these considerations have not been taken into account. It has simply been assumed that these air brakes are also engaged whenever the dynamic brakes are utilized

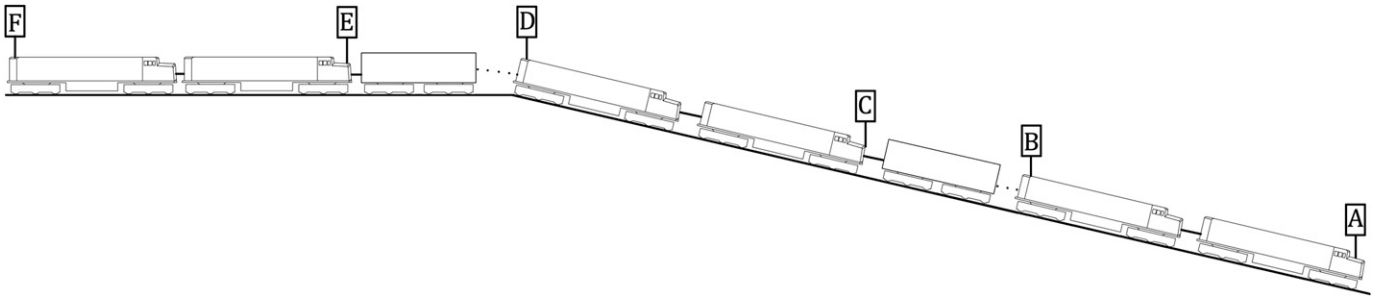

Fig. 3. Representative train and tracked points for kinematics modeling.

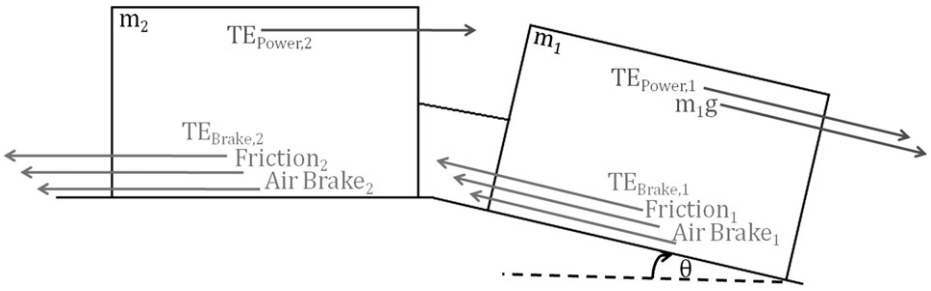

Fig. 4. Force balance acting on representative connected two-mass system.

and provide a total braking power equal to 2.2 times that provided by the tractive effort braking. The multiple 2.2 was an assumed value generated during development of the kinematics and notching model for safe operation on the steepest grades in the freight route. Thus, the air braking power was calculated as

$$\text{Air Brake}_{\text{Max},i} = \frac{L_i \cdot 3.5\text{MW} \cdot 2.2}{V} \tag{5}$$

These three forces represent the forces the locomotive engineer can control. The remaining two forces are not controlled: the friction of the wheels rolling on the tracks and the pull of gravity acting on the train. The first of these always acts in the direction opposing motion; depending on whether the grade is positive or negative for a section of the train, the gravity force can either act in the direction of the train's motion or against it. The formulations of these forces are

$$\text{Friction}_i = \mu m_i g \cdot \cos\theta_i \tag{6}$$

$$\text{Gravity}_i = m_i g \cdot \sin\theta_i \tag{7}$$

where μ is the dynamic coefficient of friction for steel on steel, taken to be 0.001, g is the acceleration due to gravity, and θ_i is the angle corresponding to the grade experienced by mass i.

Standard kinematic expressions provided the description for the effect of these forces on the train and the location of the leading locomotive (point A in Fig. 3) at the end of the timestep. The calculations made were thus

$$\sum_{m_1,m_2} F = (m_{1+}m_2) \cdot a \tag{8}$$

$$V_{t+\triangle t} = V_t + \Delta t \cdot a \tag{9}$$

$$s_{A,t+\Delta t} = s_{A,t} + V_t \cdot t + \frac{1}{2} a \cdot \Delta t^2 \tag{10}$$

where F represents the forces previously described, a is the train's acceleration, subscript t denotes a value at the beginning of the timestep, Δt is the length of a timestep, and s_A represents the position of the train's leading edge.

Evaluation of the tractive effort and air braking required simulation of a locomotive engineer's decision-making process in setting the appropriate notches. Thus, a set of nested decisions was developed to simulate this process. Inherent in this logic were some basic rules. Ideal maximum and minimum train velocities were 60 and 10 miles per hour, respectively (26.82 and 4.47 m per second); power and brake notching had to progress one notch at a time, and the train could only be in one of powering or brake mode in a timestep; notch zero on power and braking represented an idle setting at 25% of rated system power, but with power dissipated instead of supplied to the wheels; grade and instantaneous acceleration should influence the decision process; while kinematics were based on the current location of the train, notching was based on engineer's sight 1 mile ahead of the train; changes to notch settings should not oscillate excessively and should not follow each other too rapidly; the notch settings, as compared to full rated power should provide the following power and braking levels:

0: Power: 25%- Idle (No Power to Motors); Brake: 0%
1: Power and Brake: 25%
2: Power and Brake: 30%
3: Power and Brake: 38%
4: Power and Brake: 47%
5: Power and Brake: 60%
6: Power and Brake: 72%
7: Power and Brake: 85%
8: Power and Brake: 100%

The overall logic is shown in Fig. 5, with the result of the final decision in each path indicating the power or brake notch change. In the figure, line formats indicate groups of paths that lead to the same notch change decision. All decisions without a "No" path resulted in maintaining both the power and brake notches (shown as "Maintain N, NB"); these paths have been left out of the figure for the sake of clarity. In brief, the first column of decisions under "V > VMax" addresses times when the train is exceeding its speed limit. The second column, under "V < VMin" handles a similar set of decisions when the train is below its minimum desired speed. The remainder of the logic handles cases between these two extremes. The overall goal is to maximize velocity whenever possible without exceeding the upper limit. However, doing so can potentially cause the train to rapidly switch between power and braking modes when it is near the maximum speed and the ground is relatively flat. In this situation, the train would ideally coast and only have intermittent changes in notches. Thus, much of the logic presented defines a "cushion" zone (within 85% of maximum speed on a downhill and 98% on an uphill) within which no changes are allowed. For safety, a maximum downhill acceleration of 0.03 m s^{-2} was defined within the cushion zone.

3.4. Identification of route and development of load profile

Much of the motivation for completing this work stems from the desire to provide cleaner systems that operate in ports and other high-traffic shipping areas where the geography, population density, and other factors have traditionally made pollutant and greenhouse gas emissions a particularly difficult problem. Such an area can be found in southern California, where both the South Coast Air Basin, which includes the Ports of Los Angeles and Long Beach, and the neighboring Mojave Desert Air Basin, which

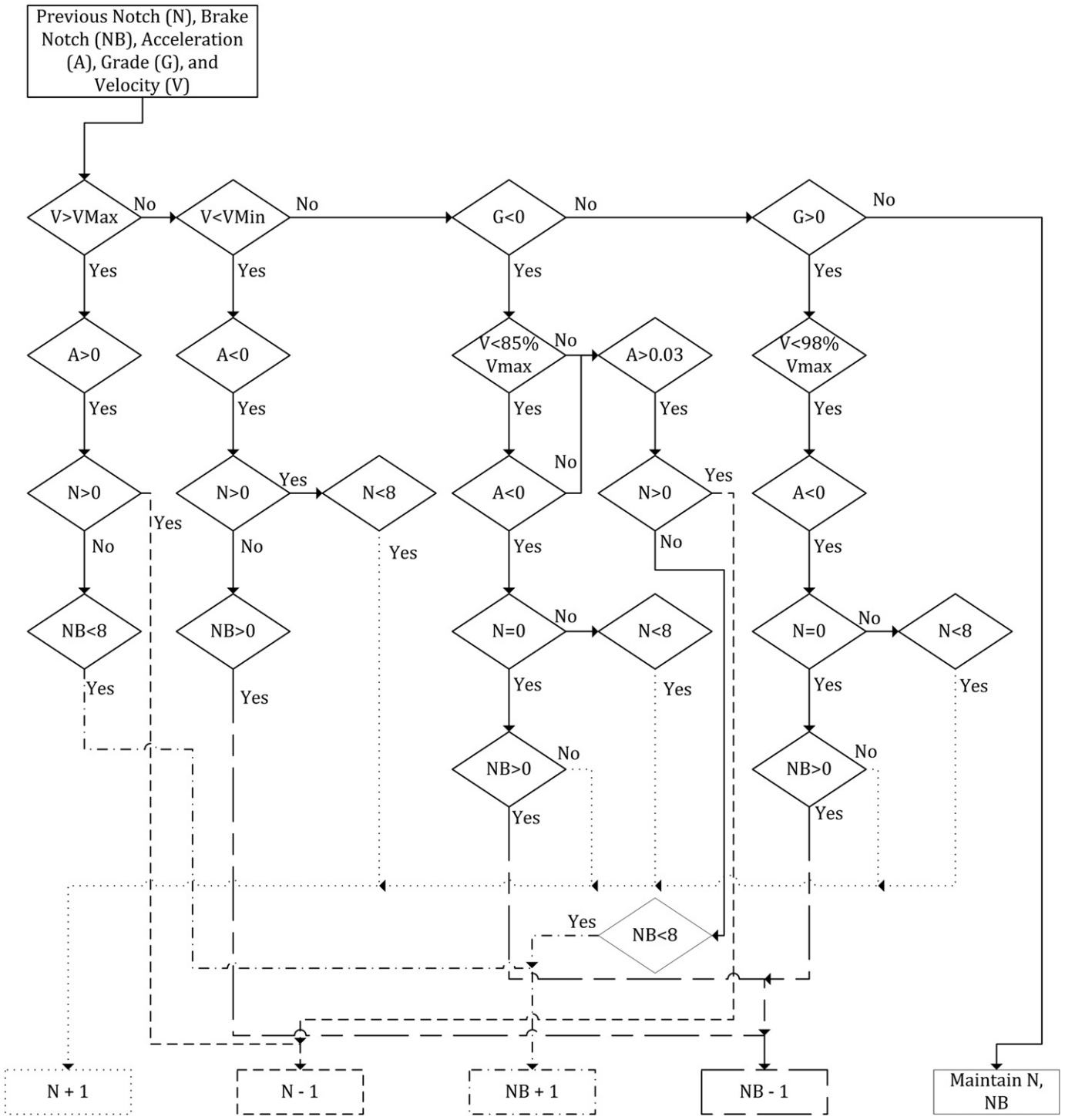

Fig. 5. Nested decision-making process for locomotive engineer notching.

includes important rail yards such as those in San Bernardino and Barstow, have high volumes of freight traffic and active programs targeting emissions reductions. Thus, a hypothetical scenario was developed for the transport of the 100-car, 6-locomotive train to move from the Ports of Los Angeles and Long Beach, through the Alameda Corridor, into the Cajon Pass, and finally ending at Barstow.

Identification of this path was achieved through ArcGIS software, which was supplied with both elevation and railroad location data provided by the United States Geological Service's National Elevation Dataset (USGS NED) [46]. Multiple sectors from the dataset were imported to the ArcGIS software, and a potential path from the ports to Barstow selected. The chosen path for simulation is shown in the map provided in Fig. 6. While it is not guaranteed that this is an actual, serviced route, it is taken as a possible representative of the type of route that a train may traverse. In addition, the Cajon Pass is known to be particularly straining for most locomotives, given its extended maximum uphill grade of

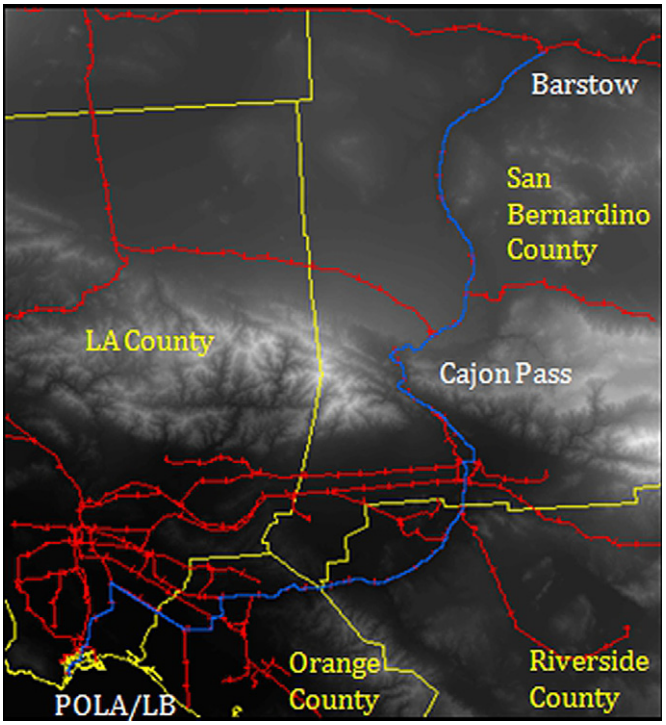

Fig. 6. Full dataset imported to ArcGIS from USGS NED; red lines indicate rail routes, yellow lines indicate county lines, gradient denotes elevation, chosen train route highlighted in blue (For interpretation of the references to color in this figure legend, the reader is referred to the web version of this article.).

approximately 3%. Using the tools available in ArcGIS, the elevation along the path was extracted and exported to a text file. This data was then smoothed by reducing the resolution to 2500 m in Excel to minimize brief, high-amplitude peaks in the extracted data, which are not expected along a rail route. The smoothed and unsmoothed elevation and grade profiles can be found in Fig. 7, where it can be seen that the maximum uphill grade is 3% and the maximum downhill grade is around 1.75%.

Simulating the train's kinematics and utilizing the elevation and grade profile along the path is preferential to utilizing a recorded engine load from an operating locomotive. It is expected that the characteristic times for various physics in the SOFC-GT system can vary from those of a diesel engine. As such, the dynamics of power delivered to the wheels would vary between the two motive power

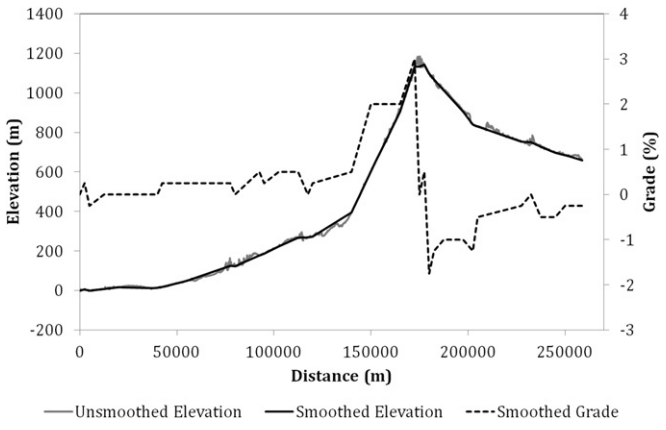

Fig. 7. Elevation and grade profiles along freight route.

systems and therefore change the timing of notch changes, even with the same notching logic. Thus, the overall load profiles may end up being similar but should not be expected to be identical. The method utilized in this work assures that the dynamic power demands are based on, and unique to, the dynamic response of the SOFC-GT.

4. System modeling results

With the test case as described above and the system model developed as reported in Part I of this work and the amendments discussed in Section 3, full system operational capability could be demonstrated in a real-world scenario. As with the results presented in Part I, it was of interest to investigate a range of fuel options which represent scenarios from the most realistic early-adoption options to more advanced and preferred fuels in the future. Thus, a scenario developing from diesel reformed offboard to LNG reformed offboard as a bridging fuel to a hydrogen future was adopted. Future work will analyze the integration of fuel reformers onboard.

4.1. System operation on diesel reformate

The major characteristics of system operation on diesel fuel reformate are presented in Fig. 8, which demonstrates the notching and system control logic had an important effect on the overall operation of the train. For example, in panel b, the previously described "cushion zones" for notching can be seen influencing operation of the train. Note also the train's velocity is able to stay within the desired bounds with the exception of the steepest section at the very peak of the Cajon Pass. This indicates that the chosen arrangement of 6 locomotives for the 100-car fully loaded train was well-suited to the application of the SOFC-GT system. Panel a provides, in the most basic of ways, a demonstration of the system's capability to perform the required task. The remaining panels demonstrate how well it accomplished this task. In panels d through g, solid black lines are the controlled parameter, dashed black the manipulated parameter, solid gray the controlled parameter's target, and dashed gray the controlled parameter's bounds. The panel b definitions are similar, with velocity solid black, grade dashed black, and velocity limits in dashed gray.

Panel a depicts the power set point changes responsible for the kinematic behavior shown in panel b, along with the corresponding dynamic system power response. Two set points are listed: the notch and the system power. In execution of the simulation, step changes in system power demand were translated into a slightly smoothed demand change in order to avoid exceedingly large derivative terms. However, the difference between the two set points was very small. The total power generated by the system closely tracked the demand for much of the simulation. The only dynamic features that caused real difficulty were those that required a rapid change from full system power (3.5 MW) to the lowest setting at notch 1 and idle of 25% system power (875 kW), or vice-versa. These dynamics are the most strenuous, so it is not surprising that they posed the greatest dynamic difficulty. These features resulted in more oscillations and longer settling times of the manipulated anode fuel flow rate and controlled system power. Aside from these excursions, there was not an excessive amount of oscillation in the system power and settling times were reasonable. One point of concern is the system power after the final load shed. Even though oscillations have mostly settled by the end of simulation, the fuel flow rate is slowly decreasing, even with the system power setting maintained for more than 3000 s.

Panel c displays the performance of the compressor as representative of the turbo-machinery over the course of operation. For

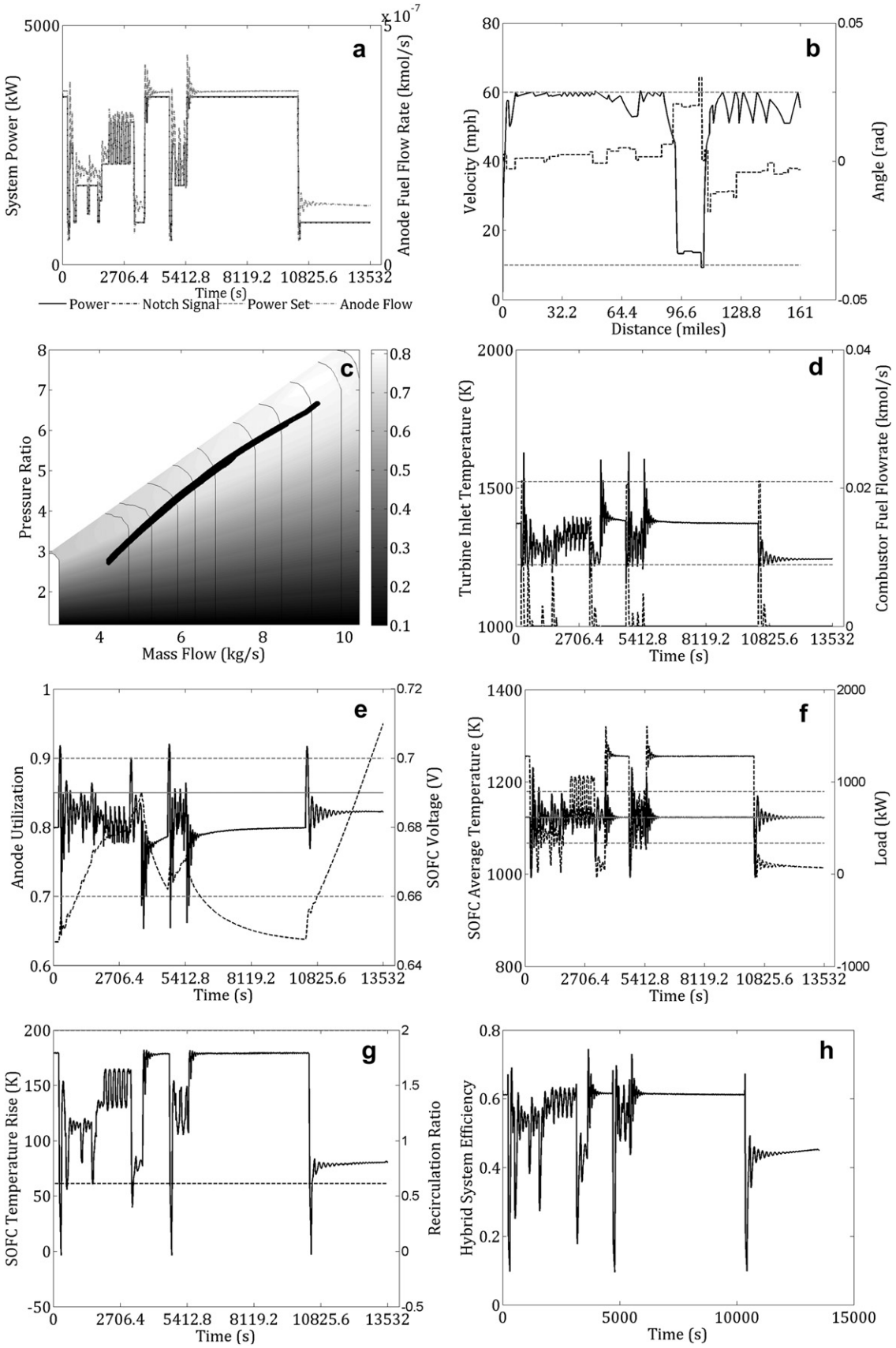

Fig. 8. System operational features in Cajon pass simulation with diesel reformate fuel.

the most part, the turbo-machinery followed a well-defined operating line with little change in pressure ratio for a given mass flow rate. However, there are some operating points where there was some variation. This is due to the dynamic variation in the combustor mass flow rate. Comparison of panels a and d shows that, during power set points between the maximum and minimum values, the combustor fuel flow underwent significant dynamic changes. Since the system power demand was also changing, the same combustor fuel flow rate occurred, briefly, for multiple system power levels. The system power setting would affect the converged pressure ratio across the turbo-machinery; thus, multiple pressure ratios could exist at different times with the same mass flow rates through the turbine and compressor. Additionally, the combustor flow rate control had some difficulty in maintaining the turbine inlet temperature within its bounds dynamically. There were not many excursions below the minimum desired value, but there were a few above the maximum, and with a significant overshoot. This was most likely due to the fact that the modeled diesel reformate contained a large amount of nitrogen; this does not react in the combustor and acts as a diluent, requiring large changes in the combustor auxiliary flow rate in order to produce a significant effect on the turbine inlet temperature.

Panel e portrays the performance of the anode fuel utilization. The direct cause of the system's final transient power response can be seen in this panel, where the SOFC voltage is still rising in an effort to bring the anode utilization down to its target value. This nearly exactly replicates an issue in the dynamic results of Part I. It was previously seen that after a large load shed, the SOFC utilization controller had difficulty in meeting the target set point and exhibited a sustained rising trend in SOFC voltage. The long duration of this transient is affected by the gain of the utilization controller (orders of magnitude lower than for the other fuels), which was found to require a low value in order to avoid deactivation of the fuel cell through attempting to impose a higher voltage than is sustainable during large transients in system power.

Previous discussions of this result, presented in Part I, seem to hold true. Namely, the high amount of CO, along with the propensity for water-gas shift to come to equilibrium within the first half of the fuel cell (shown in Fig. 9), result in difficulties maintaining high utilizations. Consider the case of low system power and therefore low anode fuel flow rate. Regardless of the system power, the goal is to maintain a constant average temperature in the fuel cell, which is accomplished fairly well in the simulation. Considering that the equilibrium of the water-gas shift and CO mole fraction are dependent only on this temperature, and not on fuel flow rate or system power, then the point in the cell along the direction of flow at which this equilibrium occurs should remain relatively unchanged. Furthermore, Fig. 9 shows that even at low power, the equilibrium point is well within the first half of the cell. However, this reaction competes with the electrochemistry. Unlike the reformation, the electrochemistry is impacted by the overall fuel flow rate and power demand; a lower system power and fuel flow result in lower electrochemical activity. Thus, with the CO concentration remaining constant regardless of system power set point, but hydrogen electrochemistry degrading with falling system power, it becomes increasingly difficult to instantaneously meet a high fuel utilization with a lower system power.

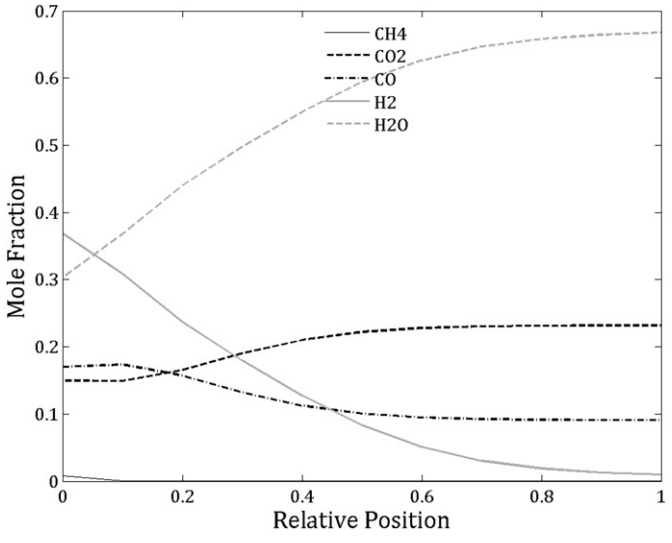

Fig. 9. Species concentration distributions in anode channel at end of diesel reformate simulation.

Another possible explanation is that during the change from a high to a low system power, when the transient change in anode fuel flow rate is not instantaneous but the power demand step is nearly-instantaneous, it is possible to have high fuel flow rates remaining in the SOFC but not very high electrochemical activity. This could lead to an instantaneously low fuel utilization, resulting in a large error signal and requiring large drops in SOFC voltage to bring utilization up to its set point. The addition of considering the CO a fuel simply makes this even more difficult as it dampens the possible effect that this change in SOFC voltage can have. In essence, since the CO is not treated as electrochemically active (but accounted for in the calculation of fuel utilization), it then behaves as a diluent, inhibiting the possible effect of any voltage change and requiring larger voltage drops than if it was not present. This reinforces the findings of Part I related to the possible role of CO electrochemistry in these systems fueled by reformates.

Panels f and g provide the last two controlled performance metrics related to the fuel cell. The average temperature does remain within its bounds for most of the simulation, but it experiences a few excursions. Larger controller gains for the SOFC average temperature can prevent these temperature excursions; however, it is at the cost of increasing the amplitude of the oscillations in the load (as well as the other manipulated and controlled variables) and the settling time. Given that the excursions were few and the not excessively large, the compromise shown in these results was considered to be acceptable. On the other hand, the SOFC temperature rise never approached its upper limit of 200 K; the chosen cathode recirculation ratio of 55% is able to provide satisfactory performance across a wide range of operational states. Finally, panel h portrays the system efficiency throughout the entirety of the simulation. During times of steady operation, the system efficiency varied between ∼61% at rated power and ∼44% at the lowest power setting.

Finally, in relation to the engine performance presented in Fig. 8, it should also be noticed that the change in combustor fuel flow rate control was successful. During simulation, there were three identifiable plateaus at rated power, with a number of dynamic power changes between them. In spite of these dynamics, once oscillations settled, the efficiency at this power setting remained constant. Moreover, it is clear from panel d that the controller was able to maintain the dual goal of a minimum turbine inlet temperature and fuel flow rate whenever it was able to do so.

As of the time of this investigation, the two major locomotive manufacturers in the USA, General Electric and Electro Motive Diesel, do not publish specific performance parameters for their engines. As a substitute for comparison, representative diesel engine operating parameters were obtained from Caterpillar (CAT) [47–49]. Table 5 summarizes the comparisons of the engine-specific performance of the SOFC-GT system versus the CAT

Table 5
Comparison of SOFC-GT system efficiency to sample Caterpillar engines.

Engine	Power (bkW)	Fuel consumption (gal-hr^{-1})	Specific fuel consumption (gal-(bkW-hr)$^{-1}$)	Thermodynamic efficiency (%)
SOFC-GT, Notch 8	3666 (3500 to motors)	175.1	0.048	61.45 (reformate), 51.00 (diesel)
SOFC-GT, Notch 1/Idle	996 (875 to motors)	62.0	0.063	42.59 (reformate), 36.18 (diesel)
Caterpillar 3516B, Max Power	1678	107.3	0.064	39.89
Caterpillar 3516B, Low Idle	309	22.21	0.072	35.49
Caterpillar C280-12 MC	4060	255.0	0.063	40.62
Caterpillar 3516C-D	2525	165.0	0.065	39.03

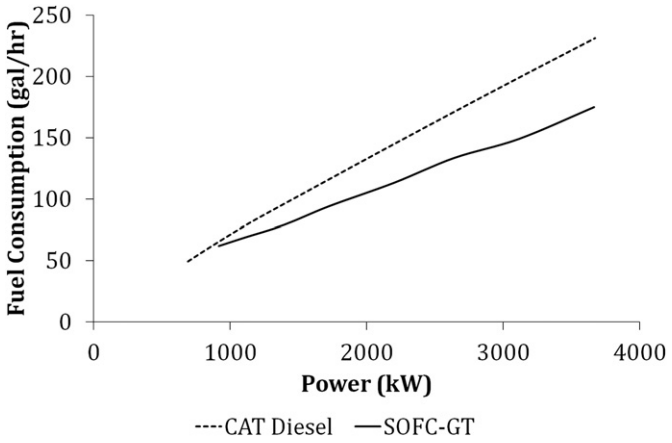

Fig. 10. Comparison of SOFC-GT and diesel engine fuel consumption across operating range.

engines. While all CAT engines specifications provided rated power data, only the 3516B provided data over its entire operating range from idle to full power. In making the comparisons shown in Table 5, it is important to be cognizant of the fact the engines utilize different fuels; the SOFC-GT analysis was based on a hexadecane reformate while the CAT engines specifications did not provide the fuel properties, but a density of 3174.6 g/gal could be estimated from the data provided. In addition, it was assumed that the LHV for diesel fuel was 141.13 MJ/gal. Even though it is known that the SOFC-GT system did not begin with this fuel, in the interest of providing a balanced comparison, the fuel consumption of the SOFC-GT system was calculated with these same values.

Table 5 provides efficiency based on the reformate stream, directly the value shown in Fig. 8, as well as efficiency for the hypothetical diesel fuel. For this diesel-based value, a reformer efficiency of 83% was assumed [50]. Importantly, this reformer efficiency is for a stand-alone reformer. In a system with a thermally integrated reformer, the efficiency impact may be more beneficial than these calculations provide. On the other hand, the single efficiency utilized is simplistic and aggregates many physical losses (pressurization, vaporization, spray losses, etc…) into a single value, which introduces some uncertainty. In the SOFC-GT results of Table 5, this reformer efficiency was utilized in the calculations of the SOFC-GT fuel consumption parameters.

At full power, on the basis of the reformate stream and the hypothetical diesel, the SOFC-GT system is significantly more efficient than the diesel engines, all of which have a full power efficiency of approximately 40%. At low power, the SOFC-GT system is slightly more efficient than the 3516B CAT engine. Over their respective operating ranges, the SOFC-GT is expected to be more efficient than the current diesel engine technology, but the SOFC-GT engine efficiency is more sensitive to the power setting than the representative CAT engine. The CAT 3516B only loses 4 points in thermodynamic efficiency over its operating range; this is a very small change in efficiency and indicates a well-designed engine. Correspondingly, the SOFC-GT engine also consumes less fuel than the diesel representatives. In terms of specific fuel consumption, the SOFC-GT at full power is again significantly preferable to the CAT engines at full power and at lowest system power is only slightly more preferred.

While Table 5 provides evidence that the SOFC-GT is the preferred technology at a given operating power, the comparison along a given route will be affected by the dependence of SOFC-GT advantage on power set point. Thus, the total and average values of fuel consumption and efficiency were derived for each engine. In the SOFC-GT case, the parameters were calculated from the assumed fuel properties for diesel and the output data of the simulation. For the CAT engine, the performance curves for the 3516B were utilized to convert the output power developed by the SOFC-GT system into corresponding instantaneous approximations of fuel consumption and efficiency for the CAT engine. The CAT 3516B engine's fuel consumption values were linearly scaled by the ratio of the SOFC-GT brake power (3666 kW) to the CAT engine brake power (1678 kW). These route-based values are displayed in Table 6, along with the expected CO_2 emission for each engine. In the case of the CAT engine, an EPA estimate of 10,217 g CO_2/gal diesel was assumed [4]. For the SOFC-GT, the total emissions were summed from the simulation recorded data.

Over the course of the Cajon Pass run, the SOFC-GT system provides approximately a 7-point increase in efficiency over the CAT engine, which is 19% of the CAT engine's efficiency. Note that this is a bit smaller than the ratio presented in Table 5 at full power, where the SOFC-GT provides an 11-point (27.5%) increase over the CAT engine. The difference relies on the effect of the load profile; notice that at low power, the SOFC-GT only provides about a 1-point (4%) efficiency gain. Thus, with instantaneous efficiencies weighted by the time at each power setting, the overall efficiency gain was only 7 points. This narrowing of the SOFC-GT advantage at low power is displayed in Fig. 10, in terms of the fuel consumption rate for each engine as a function of power. The efficiency comparisons carry over directly to the fuel consumption. By all fuel consumption measures, the SOFC-GT consumes 82% of the fuel that the CAT diesel engine is projected to, saving approximately 105

Table 6
Comparative performance of SOFC-GT system and Caterpillar engine over Cajon route.

Engine	Average fuel consumption (gal-hr^{-1})	Average specific fuel consumption (gal-(bkW-hr)$^{-1}$)	Total fuel consumption (gal)	Total CO_2 emitted (kg)	Average thermodynamic efficiency (%)
SOFC-GT	126.1	0.054	474.4	5565	54.67 (reformate), 45.38 (diesel)
Caterpillar 3516B, Scaled to 3666 bkW Max	154.15	0.067	579.9	5925	38.15
SOFC-GT Advantage	18%	19%	18%	6%	43% (reformate), 19% (diesel)

gallons per locomotive over the course of the Cajon Pass route; the entire train saves 633 gallons for the route. This represents the possibility for a nearly 20% savings in the rail operators' fueling costs, assuming the Cajon Pass route is at least a representative route.

From Table 6, the total CO_2 emitted over the route does not appear to provide a large savings; only a 6% savings from the CAT engine's projected performance is expected. However, the comparison is not direct. The SOFC-GT value is calculated from summing the CO_2 emissions in the output data of the simulation, which is based on a different fuel composition than the hypothetical diesel utilized in the remaining calculations (the composition of which is unknown). In fact, the average CO_2 emission rate from the SOFC-GT simulation is 11,732 g/gal, much higher than the representative value used for the CAT engine. However, the expectation is that the SOFC-GT saves just as much CO_2 as it does fuel, since CO_2 emissions are largely engine-independent and a property of solely the fuel (discounting the effects of incomplete combustion, engine leaks, etc.). As an illustrative alternative to the value presented in Table 6, the total fuel use in the SOFC-GT case can be recalculated based on the LHV of hexadecane, which is 128.12 MJ/gal. With this lower heat content for the fuel, the total number of gallons consumed is 522.6 gallons. With the total CO_2 provided by the simulation, the fuel's CO_2 emission rate is then 10,649 g/gallon, much closer to the EPA estimate. If the CAT engine were evaluated on this hexadecane basis, its total fuel consumption would be 638.8 gallons and its total CO_2 emissions would be 6803 kg; thus, the expected 18% savings in CO_2 would be realized. It can therefore be seen that the SOFC-GT can provide an 18% savings in all measures as long as the comparison is made equivalently.

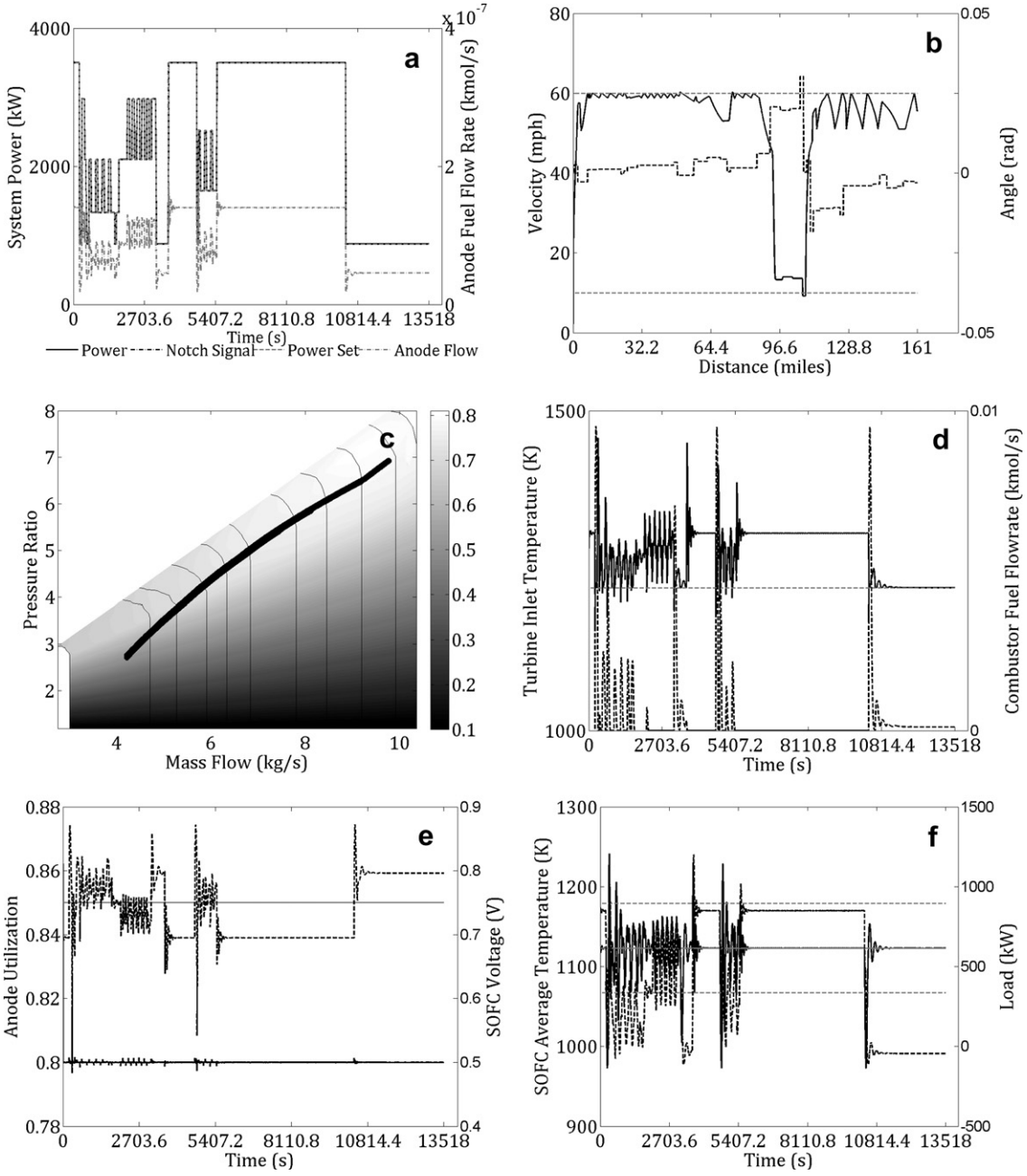

Fig. 11. System operational features in Cajon pass simulation with natural gas reformate fuel.

While the emission of CO_2 is of major concern to regulators and may become a major concern for the rail industry, it is not the only emission of concern. Currently, the EPA regulates NO_x, SO_x, unburned hydrocarbons, and CO emissions from locomotives. In this model, the kinetics of the combustion process in the auxiliary combustor were not simulated, so the actual expected emissions of these species cannot be investigated with rigorous accuracy. However, features of the system design can provide a rough estimate. Much like CO_2, SO_x emission is largely a property of the fuel; however, in the SOFC-GT system, the sulfur must be removed prior to injection into the system since the fuel cell is not tolerant to sulfur. Thus, there would necessarily be no appreciable emission of SO_x from the SOFC-GT system. However, this involves the trade-off of needing to install, utilize, and maintain the desulfurization unit previously described. Under the simulation's assumptions of complete combustion, CO and unburned hydrocarbon emissions are zero. Likewise, NO_x is not tracked. However, temperatures inside the fuel cell are too low to catalyze the formation of NO_x. In addition, the only source of these three species is the auxiliary combustor, which has a very low flow rate of unconverted fuel from the fuel cell and fresh auxiliary fuel. Combined with the high flow rate of air through the entire system, the concentration of these is expected to be low. For reference, a previous investigation into a MW-class SOFC-GT system estimated a NO_x emission of 0.04 kg/MW-hr (0.0298 g/bhp-hr) [51]. This is significantly lower than the EPA's Tier 4 guideline of 1.0 g/bhp-hr, which is to be in effect in 2015 [4].

4.2. System operation on natural gas reformate

Fig. 11 displays performance with natural gas reformate utilized as the fuel for the system. For the most part, the major features of the operational parameters seem to be similar to the diesel reformate case. The overall velocity trend and the system power settings are almost, but not quite, identical between the two fuels' simulation results. However, even though the majority of the features are so similar, there are some important differences to note as well.

Compared to the diesel reformate case, the system operating on natural gas reformate experienced significantly shorter settling times across manipulated and controlled variables, and in most measures also had lower amplitude oscillations. In addition, comparison of panel a between Figs. 8and 11 shows that the natural gas reformate case never seemed to have a significant overshoot in the system power like the diesel reformate did. Close inspection of panels a and e in Fig. 8 shows that the over- and under-shoots in system power for the diesel reformate case occurred at the times that the anode utilization violated its bounds. In the control architecture, anode utilization has greater control priority, causing system power to temporarily remain uncontrolled. Looking at the same factors in Fig. 11, the anode utilization was much more well-behaved in the natural gas reformate case and never came near its limits; therefore, the system power control was always engaged and no major excursions resulted. This contrast between the fuels suggests that increasing the amount of CO entering the cell increases the difficulty that the utilization controller has in maintaining a high set point value.

Overall, the only measure that seemed to have comparable excursions between the two fuel cases was the SOFC average temperature (the well-behaved control actions are not shown for brevity). As with diesel reformate, the gain could be tuned to remove the excursions, but at the cost of some stability. Interestingly, the excursions in SOFC average temperature are a little more severe in the case of natural gas reformate than in diesel reformate.

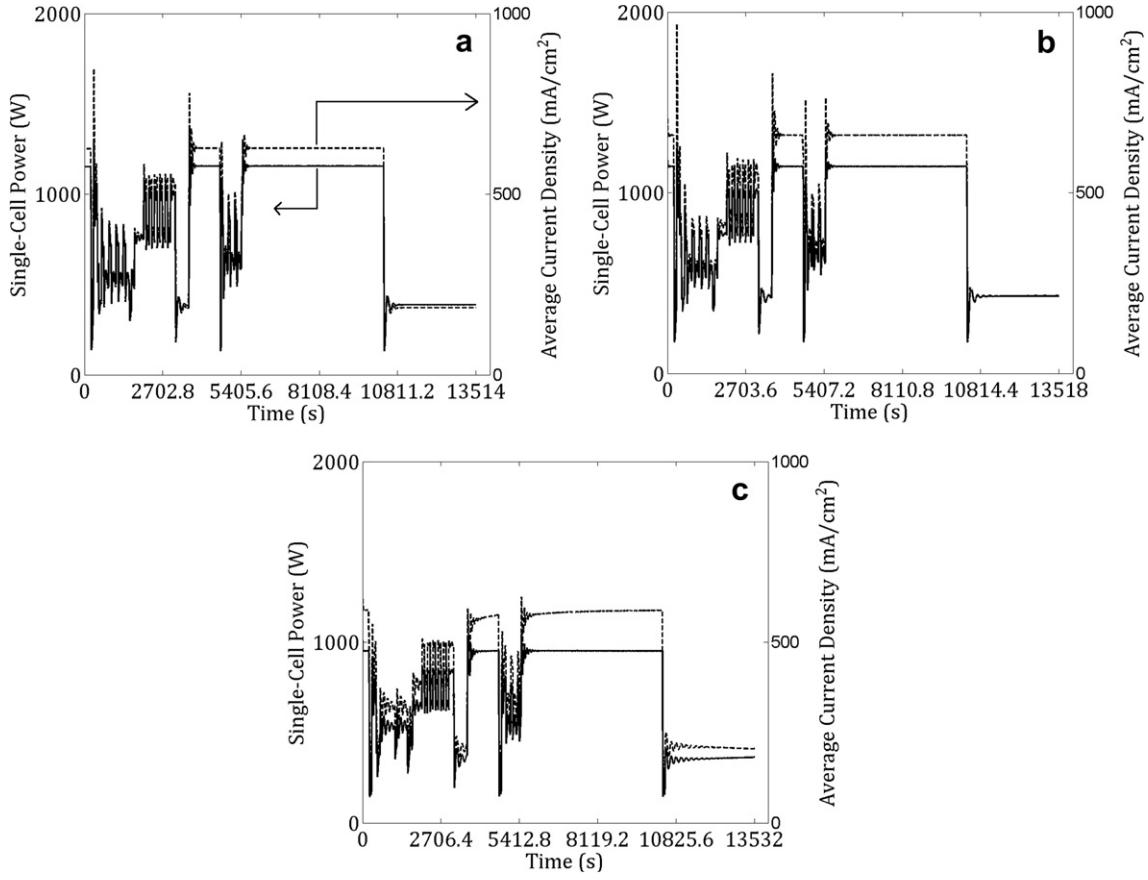

Fig. 12. SOFC power and current density for a) Diesel reformate, b) Natural gas reformate, and c) Hydrogen.

This may be due to the large amount of nitrogen present in the diesel reformate case, which acts as a heat sink, essentially damping the dynamic response of average temperature to changes in system power and SOFC heat generation.

The turbo-machinery converges along a wider operating line in the natural gas reformate case, but maintains a slightly more stable line. The increase in the operating line is constrained to the high end of the compressor map, indicating that it occurs at high system power. Again, this may be due to the nitrogen present in the fuel stream for the diesel reformate case. It may act as an additional heat sink in the fuel cell, absorbing heat that is generated, especially at high system powers. Thus, the necessary cathode air flow for the natural gas case may be greater in order to provide enough cooling potential for the cell. Additionally, Fig. 12 shows that the average current density and SOFC power-per-cell were lowest in the diesel reformate case, indicating less energy transformation and heat generation.

Finally, comparison of the system efficiencies between the two cases indicates that the natural gas reformate case is slightly advantageous, varying between approximately 64% at full power and 48% at lowest system power. Although the difference between cases is small, given the size of the system and the long routes that are typical for freight transportation by rail, this can translate to a large difference in fuel use and fuel costs for the rail operator, as well as a large difference in overall emissions.

4.3. System operation on hydrogen

Finally, the system performance on hydrogen is shown in Fig. 13. Many of the features in the hydrogen case are similar to those found

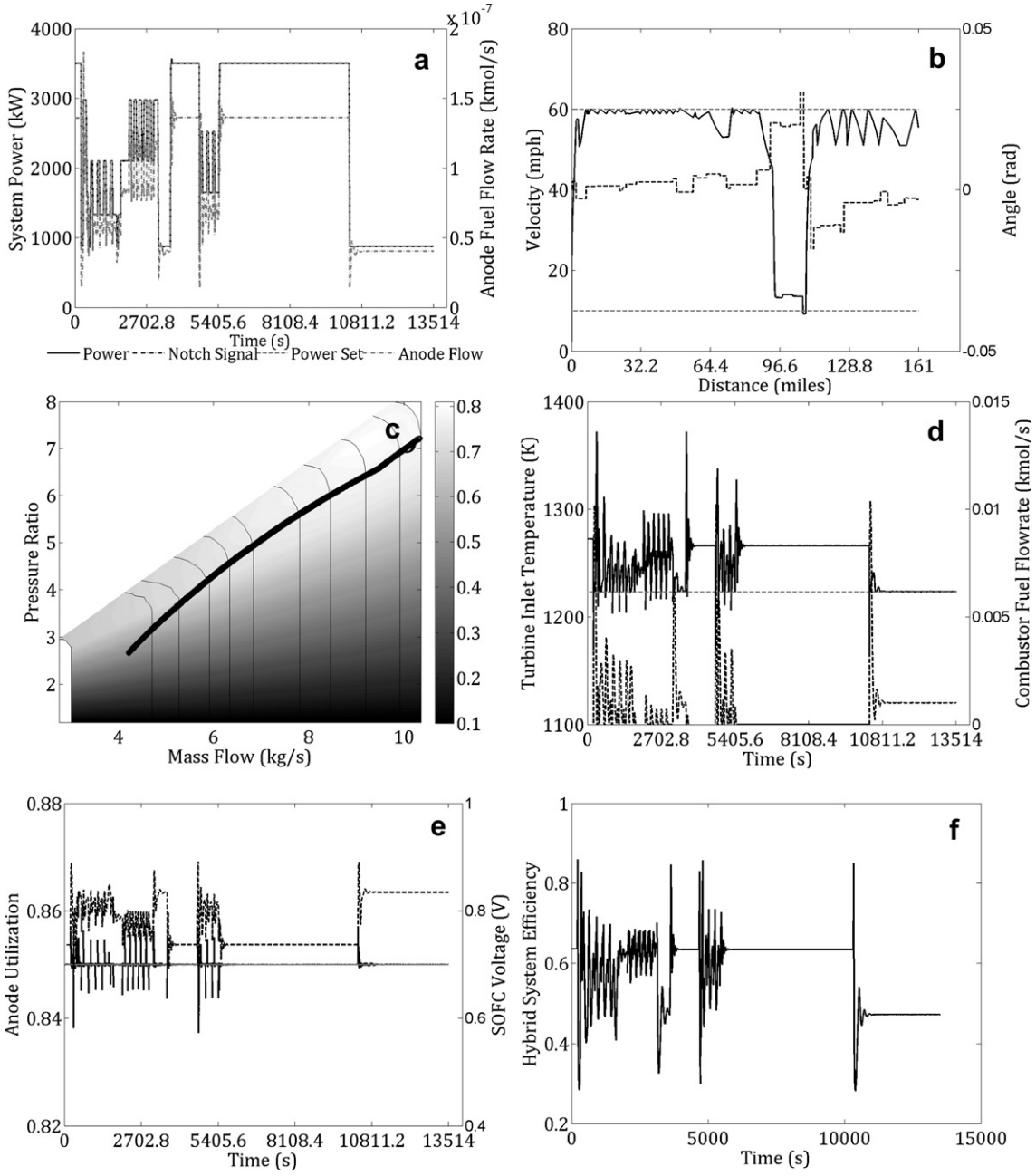

Fig. 13. System operational features in Cajon pass simulation with hydrogen fuel.

for the other two fuels. Operation on hydrogen does impart increased stability to the system operation over the entirety of the simulation, demonstrated by the significantly smaller transients and shorter settling times. This ability to come to steady-state more quickly resulted in a slightly different set of notching decisions and resulting load curve. Careful comparison of panel a across the three cases shows that early in the train's passage (beginning near 600 s of simulation time), the load changes in the hydrogen case are more dynamic. Given that the hydrogen case could reach power set points more quickly, it enabled more changes in notch settings to more closely meet the goals of the notching logic. In terms of the train's motion, the hydrogen case reached the maximum velocity a little more quickly and therefore had a slightly higher average velocity in this first part of the train's journey.

The turbo-machinery in the hydrogen case had the widest range of operation with the most stable operating line, as shown in panel c. This is most likely due to the ability of the system to quickly dampen when operating on this fuel, as the combustor flow rate transients are correspondingly faster-acting in this case than in the other two. In addition, hydrogen is a species with a high specific energy, and there were none of the diluting species in this case. Thus, even though the molar flow rate of auxiliary fuel in the combustor was comparable to the other cases, the impact on mass flow rate was necessarily smaller, resulting in the more stable operating line.

Since this fuel case did not include any CO in the inlet composition, the SOFC was able to easily meet the dynamic system power demands while maintaining fuel utilization at, or very near, 0.85 for the entirety of the simulation. Given the nature of the fuel choice, higher utilizations may be possible but may have a negative overall effect on system efficiency since it would require higher flow into the combustor. There may be an optimal fuel utilization factor for the fuel cell that can be found by further investigation. Finally, the hydrogen case proved to be nearly equivalent to the natural gas case, with a range of steady-state efficiencies between approximately 48% and 64%.

5. Summary & conclusions

5.1. Physical constraints

Although SOFC-based power systems have not yet been seriously considered as a viable technology for mobile applications, recent investigations indicate the feasibility of such a system is high. Moreover, the potential benefits of such a system contribute to the possibility of their becoming a practical reality. This has been demonstrated for the long-haul locomotive application, where space restrictions are present, but large volumes are still available for the power system. Recent advances in SOFC design bolster this potential, warranting further investigation and development, especially considering the potential impact in fuel efficiency and criteria pollutant emission that such a system can achieve.

Therefore, with proper accounting for the major system hardware and its associated balance of plant, this study demonstrates that there is sufficient motivation to pursue further study, analysis, and design of a locomotive SOFC-GT system and a demonstrable potential for this system to become a physical reality given the current state of technology.

5.2. System operational capability

While dynamic behavior proves to be more problematic for diesel fuel than the other fuel options, the system as described is capable of providing the necessary power in the target application of moving a freight train along a major rail line in Southern California. Moreover, it is able to do so in response to the modeled decision-making behavior of a locomotive engineer in order to meet their own goals regarding the motion of the train overall and not just for the power system's operation alone. All three fuel cases proved this capability at an attractive overall system efficiency, near 65% at full power depending on the fuel utilized. For the natural gas and diesel reformate cases, these high efficiencies should be understood to include an assumption that the fuel is already pre-reformed. However, it has also been demonstrated that even with a conservative estimate for a stand-alone reformer's efficiency, the overall system efficiency can be significantly higher than a typical diesel engine. Future investigations will analyze a system architecture that integrates the reformation units in order to minimize the thermodynamic losses. The combination of high system efficiency, improved specific fuel consumption, and savings in CO_2 over the course of operation are highly-desirable attributes for a prime mover in a heavy industrial application such as freight transportation. Overall, it is expected that a rail operator could realize an 18% savings in fuel use and CO_2 emission with a train like the one described in this work, operating along the chosen path, which includes a particularly challenging geographical feature along its route.

From the perspective of the system performance potential, the SOFC-GT is a strong candidate system for the freight locomotive application. With the findings demonstrated in this investigation, further development of the system in terms of optimizing system theoretical design and moving toward demonstration of physical test systems will provide further insights into the benefits of the system as well as the challenges that may need to be overcome for its eventual physical integration into the current locomotive freight system.

Acknowledgments

This material is based upon work supported under a National Science Foundation Graduate Research Fellowship. Any opinions, findings, conclusions, or recommendations expressed in this publication are those of the author and do not necessarily reflect the views of the National Science Foundation.

The statements and conclusions in this Report are those of the contractor and not necessarily those of the California Air Resources Board. The mention of commercial products, their source, or their use in connection with material reported herein is not to be construed as actual or implied endorsement of such products.

This report was prepared as a result of work sponsored, paid for, in whole or in part, by the South Coast Air Quality Management AQMD (AQMD). The opinions, findings, conclusions, and recommendations are those of the author and do not necessarily represent the views of AQMD. AQMD, its officers, employees, contractors, and subcontractors make no warranty, expressed or implied, and assume no legal liability for the information in this report. AQMD has not approved or disapproved this report, nor has AQMD passed upon the accuracy or adequacy of the information contained herein.

References

[1] United States Department of Transportation, Research and Innovative Technology Administration (2009) Bureau of Transportation Statistics. 2007 Commodity Flow Survey.
[2] California Air Resources Board, Diesel Particulate Matter Exposure Assessment Study for the Ports of Los Angeles and Long Beach (2006) Sacramento.
[3] California Air Resources Board, Health Risk Assessment for the BNSF Railway San Bernardino Railyard (2008) Sacramento.
[4] Environmental Protection Agency, Technical Highlights: Emissions Factors for Locomotives (2009) Washington, DC.

[5] S.C. Davis, S.W. Diegel, Transportation Energy Data Book, twenty sixth ed. Oak Ridge National Laboratory, Oak Ridge, 2007.
[6] Environmental Protection Agency, Inventory of U.S. Greenhouse Gas Emissions and Sinks 1990–2009 (2011) Washington, DC.
[7] General Electric, The Evolution Series Locomotives: Moving Rail Power Forward (2005).
[8] G. Chen, P.L. Flynn, S.M. Gallagher, E.R. Dillen, Journal of Engineering for Gas Turbines and Power 125 (2003) 505–512.
[9] L. Salasoo, A. Kane, R.D. King, T. Richter, A.K. Kumar, H.Y. Young, in: Proceedings on the 23rd Electric Vehicle Symposium (2007) Anaheim, 2007.
[10] Frank Stodolsky, Railroad and Locomotive Technology Roadmap, US Department of Energy, Argonne, 2002.
[11] B.A. Steinberg, D.S. Scott, International Journal of Hydrogen Energy 9 (1) (1984) 101–107.
[12] W.D. Jones, IEEE Spectrum (Aug. 2006) 10–13.
[13] H.S. Murray, J.R. Huff, E.W. Gregory II, Extended Abstracts of the Electrochemical Society 82 (1982) 471.
[14] D.S. Scott, H.H. Rogner, M.B. Scott, International Journal of Hydrogen Energy 18 (3) (1993) 253–263.
[15] A.R. Miller, J. Peters, in: Proceedings of the 2006 IEEE/ASME Joint Rail Conference (2006) Atlanta, 2006.
[16] A.R. Miller, J. Peters, B.E. Smith, O.A. Velev, Journal of Power Sources 157 (2006) 855–861.
[17] A.R. Miller, K.S. Hess, D.L. Barnes, T.L. Erickson, Journal of Power Sources 173 (2007) 935–942.
[18] Solid State Energy Conversion Alliance (SECA), Office of Fuel Cell Energy Annual Report, United States Department of Energy, Washington, DC, 2007.
[19] EG&G Technical Services, I, Fuel Cell Handbook, seventh ed. U.S. Department of Energy, Morgantown, 2004.
[20] Veyo, et al., Journal of Engineering for Gas Turbines Power 124 (2002) 845–849.
[21] General Electric, GE7FDL Specs (2004).
[22] R.A. Roberts, et al., Journal of Engineering for Gas Turbines and Power 128 (2) (2006) 294–301.
[23] Kawasaki, Kawasaki Gas Turbine Generator Sets (2007).
[24] Solar Turbines, Solar 20 Gas Turbine Generator Set (2005).
[25] Jiangsu Sanji Industrial Co. Ltd, Zinc Oxide Sulfur Removal Catalyst (October 6, 2009).http://www.sanji-ind.com/productinfo.php?cid=306.
[26] Copeland, et al., Regenerating a Long-Life Zinc Oxide-Based Sorbent for Moving-Bed Reactors, TDA Research, Wheat Ridge, 1997.
[27] X. Bu, et al., Fuel Processing Technology 88 (2007) 143–147.
[28] S. Roychoundhury, et al., Journal of Power Sources 160 (1) (2006) 510–513.
[29] United States Environmental Protection Agency. Overview of EPA's Low Sulfur Diesel Fuel Programs. November 15, 2004. October 6, 2009. http://www.epa.gov/cleandiesel/presentations/overviewulsdprgrm.pdf
[30] M. Flytzani-Stephanopoulos, M. Sakbodin, Z. Wang, Science 312 (2006) 1508–1510.
[31] FuelCell Energy, Direct FuelCell DFC3000 (2007).
[32] FuelCell Energy, Kentucky Pioneer Energy LLC Integrated Gasification Combined Cycle Project 2 MW Fuel Cell Demonstration, FuelCell Energy, Danbury, 2006.
[33] W. Winkler, H. Lorenz, Journal of Power Sources 106 (2002) 338–343.
[34] T. Suzuki, T. Yamaguchi, Y. Fujishiro, M. Awano, Journal of Power Sources 160 (2006) 73–77.
[35] T. Suzuki, T. Yamaguchi, Y. Fujishiro, M. Awano, Journal of the Electrochemical Society Vol. 5 (2006) A925–A928 153.
[36] T. Suzuki, Y. Funahashi, T. Yamaguchi, Y. Fujishiro, M. Awano, Journal of Power Sources 171 (2007) 92–95.
[37] T. Suzuki, T. Yamaguchi, Y. Fujishiro, M. Awano, Journal of Power Sources 163 (2007) 737–742.
[38] T. Suzuki, Y. Funahashi, T. Yamaguchi, Y. Fujishiro, M. Awano, Electrochemical and Solid-State Letters 10 (8) (2007) A177–A179.
[39] Y. Funahashi, T. Shimamori, T. Suzuki, Y. Fujishiro, M. Awano. Fabrication and characterization of components for cube shaped micro tubular SOFC bundle, Journal of Power Sources 163 (2007) 731–736. Fytzani-Stephanopoulos, et al. Regenerative Adsorption and Removal of H2S from Hot Fuel Gas Strea6ms by Rare Earth Oxides. Science 312(5779) (2006) 1508–1510.
[40] T. Suzuki, Y. Funahashi, T. Yamaguchi, Y. Fujishiro, M. Awano, Journal of Power Sources 175 (2008) 68–74.
[41] K. Eguchi, T. Setoguchi, T. Inoue, H. Arai, Solid State Ionics 52 (1992) 165–172.
[42] D. Hirabayashi, A. Tomtima, T. Hibino, M. Nagao, M. Sano, Solid-State Letters 7 (2004) A318–A320.
[43] Y. Liu, M. Mori, Y. Funahashi, Y. Fujishiro, A. Hirano, Electrochemistry Communications 9 (2007) 1918–1923.
[44] Y. Fujishiro, K. Mamamoto, R.V. Mangalaraja, M. Awano, Key Engineering Materials 317-318 (2006) 909–912.
[45] Union Pacific. Allowable Gross Weight. Union Pacific. http://www.uprr.com/aboutup/maps/grossweight.shtml. (accessed 11.07.11.).
[46] United States Department of the Interior. 0. http://ned.usgs.gov/. August, 2006. (accessed 11.07.11.).
[47] Caterpillar, Locomotive 3516B Engine (2000).
[48] Caterpillar. "Caterpillar Marine Power Systems: 3516C." Caterpillar. http://marine.cat.com/cat-3516C. (accessed July 11.07.11.).
[49] Caterpillar. "Caterpillar Marine Power Systems: C280–12." Caterpillar. http://marine.cat.com/cat-C280-12. (accessed July 11.07.11.).
[50] I. Kang, J. Bae, S. Yoon, Y. Yoo, Journal of Power Sources 172 (2007) 845–852.
[51] W.L. Lundberg, S.E. Veyo, M.D. Moeckel, Journal of Engineering for Gas Turbines and Power 125 (2003) 51–58.